

Fabrication, characterization and photocatalytic properties of CdS nanoparticles modified by N-doped TiO₂ NTs

DAWEI GAO^{1,*}, CHUNXIA WANG¹, YU JIAN¹, WEIWEI LI¹, PENGYU DONG²

¹College of Textiles and Clothes, Yancheng Institute of Technology,
Yancheng 224051, P.R. China

²Key Laboratory for Advanced Technology in Environmental Protection of Jiangsu Province, Yancheng Institute of
Technology, Yancheng 224051, P.R. China

Highly ordered TiO₂ nanotube arrays (TiO₂ NTs) were prepared by anodic oxidizing method on a surface of Ti substrate. Fabrication of nitrogen-doped TiO₂ nanotube arrays (N-TiO₂ NTs) was carried out by immersion in ammonia solution. CdS nanoparticles loaded N-doped TiO₂ nanotube arrays (CdS/N-TiO₂ NTs) were obtained by successive ionic layer adsorption and reaction (SILAR) technique. The samples were characterized by X-ray diffraction (XRD), X-ray photoelectron spectroscopy (XPS), field emission scanning electron microscopy (FE-SEM), transmission electron microscopy (TEM), high resolution transmission electron microscopy (HRTEM), photoluminescence (PL) emission spectra and ultraviolet-visible (UV-Vis) diffuse reflectance spectroscopy (DRS). The results indicate that the TiO₂ nanotube diameter and wall thickness are 100 nm to 120 nm and 20 nm to 30 nm, respectively. Moreover, the morphology and structure of the highly ordered TiO₂ NTs are not affected by N-doping. Furthermore, CdS nanoparticles are evenly distributed on the surface of TiO₂ NTs. Finally, the photocatalytic activity of CdS/N-TiO₂ NTs was evaluated by degradation of MO under visible-light irradiation. Compared with TiO₂ NTs, N-TiO₂ NTs, CdS/N-TiO₂ NTs exhibited enhanced photocatalytic properties, and the highest degradation rate of CdS/N-TiO₂NTs could reach 97.6 % after 90 min of irradiation.

Keywords: *TiO₂ nanotube arrays; N dopants; CdS nanoparticles; visible light; photocatalysis*

1. Introduction

Photocatalytic degradation of various organic and inorganic pollutants using semiconductor nanopowders has been intensively investigated [1–3]. Among various photocatalysts, TiO₂ has been one of the most promising materials due to its non-toxicity, chemical inertness, photocatalytic activity and low cost [4, 5]. However, the small surface area, poor photoresponse under visible light and the high rate of photogenerated electron/hole pair recombination among TiO₂ nanoparticles are the main factors limiting further improvement of its photocatalytic efficiency.

Recently, varieties of TiO₂ nanostructures, including nanorods, nanowires, nanobelts and nanotubes have been fabricated for degradation of organic pollutants. Among them, the TiO₂ nanotube arrays (TiO₂ NTs) prepared by anodic oxidation

method can be easily recovered and reused in waste water treatment. The tubes perpendicular to the Ti substrate form a Schottky-type contact and provide a unidirectional electric channel for the transport of photogenerated electrons [6]. Moreover, the aligned nanotube structure can reduce reflection of the light because of multiple radiation scattering by the nanotube walls [7].

However, due to its wide band gap (3.2 eV and 3.0 eV for anatase and rutile phases, respectively), the photocatalytic activity of TiO₂ is only limited in the UV region which is about 4 % to 5 % of the solar energy. Considerable attempts have been made to improve the visible light absorption of TiO₂ by the substitutional non-metallic doping (N [8], C [9], S [10], etc.), novel metallic doping (Ag [11], Pt [12], Au [13], etc.) or depositing narrow-gap semiconductor materials (CdS [14], CdSe [15], CdTe [16], etc.). Among different non-metal dopants, N-doping attracts much attention due to its atomic size comparable with oxygen,

*E-mail: gdw8668@163.com

small ionization energy, metastable center formation and its stability [17]. Moreover, N-doping is considered as an ideal dopant due to the obvious reduction of the band gap of the TiO₂ [18–20]. However, oxygen vacancies are usually generated by doping of N into the lattice of TiO₂, which act as recombination centers and decrease the photocatalytic efficiency. To solve this problem, N-doped TiO₂ modified with chalcogenide semiconductor was proposed. Compared with other semiconductors, CdS with a narrow band gap (2.4 eV) and relatively high absorption coefficient in the visible region is highly desirable for the use in photocatalysis and solar cells [21, 22]. The photogenerated electrons would move from CdS to TiO₂ to restrain charge recombination in TiO₂-CdS system, thereby, improving the photocatalytic activity of TiO₂. Herein, we report a facile method to fabricate CdS nanoparticles modified N-doped TiO₂ nanotube arrays. The morphologies, structures, compositions and photocatalytic properties of as-prepared materials were studied.

2. Experimental

2.1. Preparation of CdS/N-TiO₂ NTs

Ethanol, acetone, HNO₃, HCl, HF, NH₄F, CdCl₂, Na₂S, and ethylene glycol were purchased from Sinopharm Chemical Reagent Co., Ltd. All reagents were used without further purification.

A two-step anodization method was used to prepare TiO₂ NTs on Ti substrate [6]. Titanium foils (99.8 % purity) with a size of 15 mm × 15 mm × 0.1 mm were ultrasonically cleaned for 10 min in water, acetone and ethanol, respectively. Then the titanium foils were anodized under 50 V for 1 h in ethylene glycol solution containing 0.5 wt.% NH₄F and 2.5 vol.% H₂O. The as-formed TiO₂ NTs layer was peeled off by ultrasonication in deionized water to expose the Ti substrate. The second-step anodization was carried out in the mentioned electrolyte for 2 h. After anodic oxidation, the samples were rinsed with ethanol for 5 min. The as-prepared samples were immersed in 1 M NH₃·H₂O solution for 12 h and annealed in a muffle furnace under ambient atmosphere at 450 °C for 1 h to obtain the TiO₂ nanotubes [8].

CdS nanoparticles were deposited on N-TiO₂ NTs using SILAR process [14]. The as-prepared N-TiO₂ NTs were dipped into a 0.1 M CdCl₂ aqueous solution for 1 min, rinsed with deionized water, and then dipped for another 1 min into a 0.1 M Na₂S aqueous solution, and rinsed again with deionized water. The samples were denoted as CdS/N-TiO₂ NTs.

2.2. Characterization

The morphologies of the samples were studied by field-emission scanning electron microscopy (FE-SEM, JOEL, JSM-6700F), and transmission electron microscopy (TEM, Philips, and CM120). The crystal structure of the samples was characterized by X-ray diffraction technique (MAC Science Co., Ltd. MXP 18 AHF, CuKα, λ = 0.15418 nm). The surface chemical composition of the samples was analyzed by X-ray photoelectron spectroscopy (XPS, PHI Quantum 2000) with AlKα radiation source. All the binding energies were referred to the C1s peak at 284.8 eV of the surface adventitious carbon. The photoluminescence (PL) emission spectra of the samples were measured at room temperature by Fluoromax-4 spectrofluorometer (USA) using 300 nm xenon lamp excitation. The UV-Vis diffuse reflectance spectra (DRS) of the samples were recorded by a UV-Vis spectrophotometer (UV-2550, Shimadzu). BaSO₄ was used as a reflectance standard in the wavelength range of 300 nm to 800 nm.

2.3. Photocatalytic activity test

The photocatalytic activity of the as-prepared samples was evaluated by photocatalytic decomposition of 30 mL methyl orange (MO, 10 mg/L) aqueous solution under 250 W xenon lamp. The cut-off filters were used to obtain visible light (λ > 400 nm). The suspension was constantly stirred in the dark for 15 min to achieve adsorption-desorption equilibrium. The concentration change of MO was monitored by determining the UV-Vis adsorption at 464 nm every 15 min. After measurement, the photo-degradation experiments were continued on the sample as mentioned above.

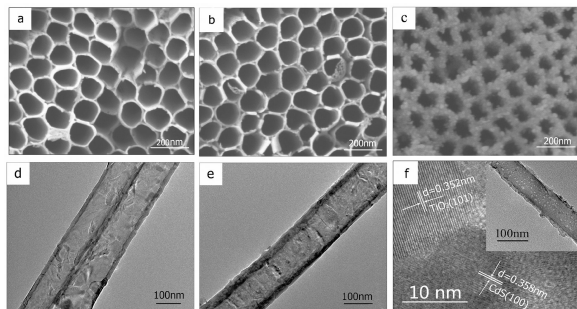


Fig. 1. SEM, TEM and HRTEM images of (a) and (d) TiO_2 NTs, (b) and (e) N- TiO_2 NTs, (c) and (f) CdS/N- TiO_2 .

3. Results and discussion

Fig. 1 shows typical SEM and HRTEM images of both as-prepared samples. As shown in Fig. 1a and Fig. 1d, the samples consist of a well-aligned and vertical tubular structures with a diameter of 110 nm to 130 nm and wall thickness of 15 nm. Fig. 1b and Fig. 1e indicate that the well-ordered porous structure was preserved, suggesting that N-doping did not damage the ordered TiO_2 nanotube arrays structure. Fig. 1c shows that the surface of the nanotubes has been successfully coated with a relatively uniform layer of CdS nanoparticles. Typical HRTEM and TEM (inset) images of CdS/N- TiO_2 NTs are shown in Fig. 1d. The HRTEM image displays the lattice fringe with lattice spacing of 0.358 nm, corresponding to the (1 0 0) lattice planes of CdS, as noted in Fig. 1d, what is in accordance with the results of XRD. The lattice with d spacing of 0.352 nm, corresponding to the (1 0 1) plane of TiO_2 can be found from HRTEM images [23].

Fig. 2 shows the XRD patterns of TiO_2 NTs, N- TiO_2 NTs and CdS/N- TiO_2 NTs. The patterns display two diffraction peaks at 40.5° and 53.2° , corresponding to (1 0 1) and (1 0 2) crystal faces of Ti substrate, respectively. The characteristic peaks at 25.5° , 37.1° , 37.8° , 48.2° , 54.1° , 55.2° , 62.9° , 68.8° and 70.6° can be identified as the crystal planes of (1 0 1), (0 0 4), (1 1 2), (2 0 0), (1 0 5), (2 1 1), (2 0 4), (1 1 6) and (2 2 0) planes of anatase TiO_2 (JCPDS Card No. 21-1272). The characteristic peaks that appeared at the 26.5° and 43.8° can be

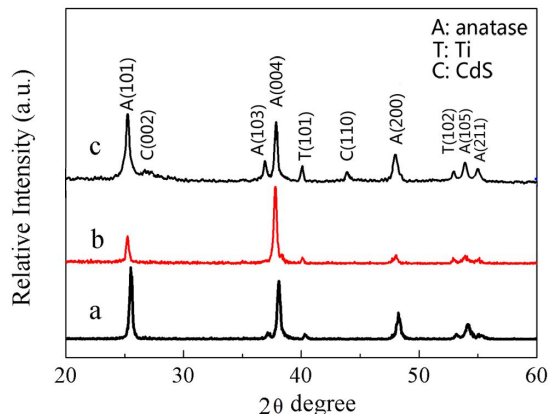


Fig. 2. XRD patterns of TiO_2 NTs (a), N- TiO_2 NTs (b), CdS/N- TiO_2 (c).

indexed as the CdS hexagonal structure with crystal faces of (0 0 2) and (1 1 0), respectively (JCPDS Card No. 41-1049).

The average particle size was calculated using the Scherrer equation:

$$d = 0.89\lambda / \beta \cos \theta \quad (1)$$

where d is the crystal size, k is the constant (0.89), λ is the X-ray wavelength (1.54 \AA), β is the full width at half maximum (FWHM) of the peaks, θ is the diffraction angle. The crystallite sizes of TiO_2 NTs, N- TiO_2 NTs and CdS/N- TiO_2 NTs, which have been calculated using anatase (1 0 1) diffraction peak, are 31.22 nm, 27.92 nm and 28.02 nm, respectively. It shows that CdS modification had little effect on the crystallite sizes of TiO_2 , while the growth of TiO_2 crystallites during calcination was strongly inhibited by N-doping.

The surface element composition and chemical states of CdS/N- TiO_2 NTs were analyzed by XPS, as shown in Fig. 3. Fig. 3a demonstrates the N1s XPS spectrum of the CdS/N- TiO_2 NTs. The N1s peak at 399.8 eV can be attributed to the oxidized nitrogen in the form of O-Ti-N linkage instead of molecularly chemisorbed N species on the surface of TiO_2 NTs [16, 17]. In Fig. 3b, the binding energies of 458.2 eV and 464.4 eV are ascribed to the peaks of Ti 2 $p_{3/2}$ and Ti 2 $p_{1/2}$, respectively, which are ascribed to the titanium lattice in TiO_2 with a 2 p_3 binding energy of Ti (IV) ion. The peak shift

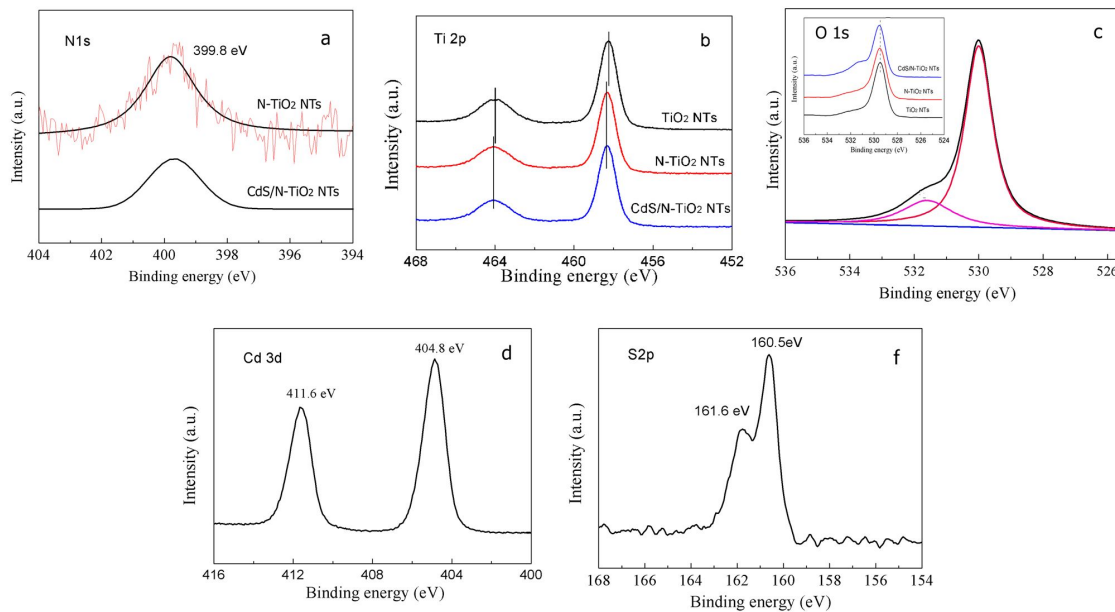


Fig. 3. XPS high resolution spectra of N1s (a), Ti2p (b), O1s (c), Cd 3d (d) and S 2p (e).

may contribute to the doping of N into the TiO₂ lattice. The O1s XPS spectrum in Fig. 3c can be divided into two peaks centered at 531.1 eV and 530.0 eV, respectively. Besides the presence of substitutional N, it further confirms the formation of the O–Ti–N structure. The XPS spectrum of CdS3d in Fig. 3d shows that the 3d_{3/2} and 3d_{5/2} signals are located at 411.6 eV and 404.8 eV, respectively. The splitting of the 3d doublet is 6.8 eV which indicates that the CdS loading on the TiO₂ surface exists as a form of Cd²⁺ [24]. As shown in Fig. 3e, binding energies of 160.5 eV and 161.6 eV are ascribed to the peaks of S 2p_{3/2} and S 2p_{1/2}, respectively. The 2p splitting of 1.1 eV between S 2p_{3/2} and S 2p_{1/2} confirms the S²⁻ state [25].

Herein, PL analysis was used to reveal the efficiency of charge carrier trapping, transfer, and separation and to investigate the fate of photogenerated electrons and holes in semiconductors [29]. Fig. 4 shows a comparison of fluorescence emission spectra of TiO₂ NTs, N-TiO₂ NTs and CdS/N-TiO₂ NTs within the range of 350 nm to 550 nm. It can be seen that all the samples show the similar PL spectra with peaks centered at 400 nm and 470 nm, respectively. The peak located at about 400 nm is related to the electron transi-

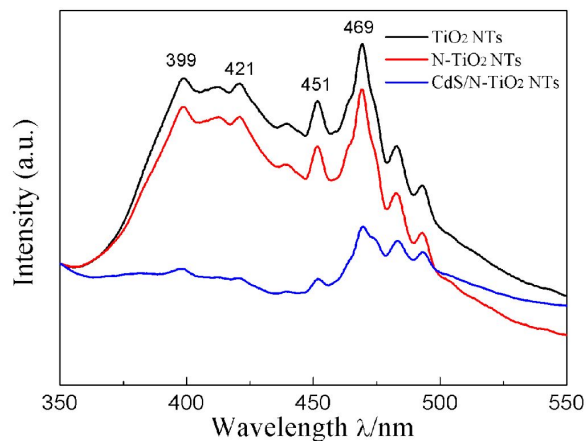


Fig. 4. Photoluminescence emission spectra of the samples.

tion from the valence band to conduction band, so-called self-trapped excitons, while the peak at 470 nm can be ascribed to surface oxygen vacancies located at the surface of TiO₂ NTs. From the results, the PL intensity of N-doped TiO₂ NTs is lower than that on TiO₂ NTs, indicating that N-doping markedly enhances the charge separation of photogenerated carriers of TiO₂ NTs. In comparison with N-TiO₂ NTs, the intensities of the PL

emission of the CdS/N-TiO₂ NTs samples are much lower, which indicates relatively lower recombination of excited electrons and holes. The peak intensity of CdS/N-TiO₂ nanotubes decreased significantly compared with N-TiO₂ nanotubes. This may be ascribed to the heterojunction existing between CdS and TiO₂ NTs due to Cd-O bonds that the electrons photoinduced on the surface of CdS particle can transfer easily from the CB of CdS to that of TiO₂ NTs via the well-developed hetero TiO₂-CdS interface which hinders the direct electron-hole recombination [26].

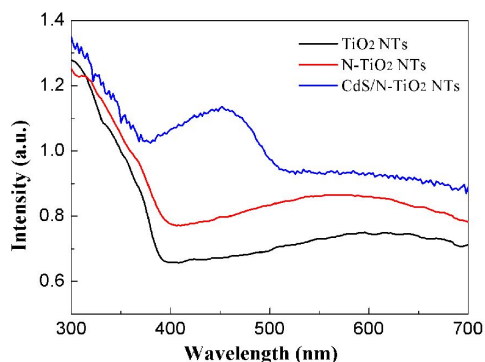


Fig. 5. UV-Vis absorption spectra of the samples.

Fig. 5 shows the UV-Vis absorption spectra of the samples. All the samples were of the same size. For the TiO₂ NTs with the band-gap energy of 3.2 eV, the intrinsic absorption in the wavelength region is below 400 nm. The absorption of TiO₂ NTs in the visible region can be assigned to scattering of light caused by pores or cracks of the nanotube arrays [27]. Moreover, the characteristic absorption edge for N/TiO₂ NTs shows a red-shift and exhibits stronger absorption. This is due to the 2p orbitals of N atom interacting with O atoms, which demonstrates an effective charge transfer between the dopant and the conduction or valence band [28]. Further, CdS/N-TiO₂ NTs sensitized with CdS nanoparticles, show apparent enhancement of absorption in visible region because of the surface plasmon resonance of CdS nanoparticles deposited on the TiO₂ NTs which suggests that the improvement of photocatalytic efficiency in the visible region could be possible [29].

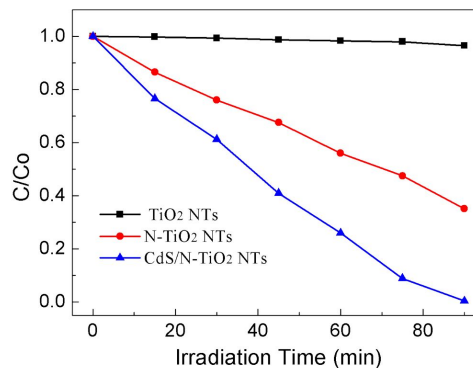


Fig. 6. Variation of MO concentration against irradiation time for TiO₂ NTs, N-TiO₂ NTs, and CdS/N-TiO₂.

The photocatalytic activity of the as-prepared samples was then investigated. Fig. 6 shows the degradation rate of MO under visible light for 90 min for different samples. It is obvious that the TiO₂ NTs and CdS/N-TiO₂ NTs have the lowest and the best photocatalytic ability, respectively, with 3.5 % and 97.6 % decomposition of the MO after 90 min under visible light. The degradation rate for N-TiO₂ NTs after 90 min increased to 64.9 % because of the enhancement of separation and efficient transferring of the photogenerated carriers after N-doping [30, 31]. The larger surface areas after loading of CdS nanoparticles enhanced the light harvesting and the separation efficiency of the electron-hole pairs. Besides, the enhanced photocatalytic properties for the CdS/N-doped TiO₂ NTs in visible region may also be attributed to the facilitated formation of active radicals, LSPR effect and synergistic effect between CdS nanoparticles and N-TiO₂ NTs. Thus, the CdS/N-TiO₂ NTs demonstrated the highest photocatalytic activity towards the degradation of MO, which was consistent with the fluorescence quenching effect revealed by PL spectra in Fig. 4.

4. Conclusions

In summary, the nanostructure and composition of a CdS/N-TiO₂ NTs can be designed for higher photodegradation efficiency through doping and depositing of N and CdS. Firstly, N-doped TiO₂ NTs have been successfully

fabricated directly by anodic oxidation of Ti foils, followed by ambient heat treatment of the TiO₂ NTs pre-soaked in ammonia solution. Then, CdS nanoparticles were successfully deposited on the surface of the N-TiO₂ NTs by the ionic layer adsorption and reaction technique. The tubular morphology of TiO₂ NTs was not destroyed after N-doping, and nitrogen atoms were successfully incorporated into the interstitial sites of the TiO₂ crystal lattice. In comparison with TiO₂ NTs, the photocatalytic degradation rate of CdS/N-TiO₂ nanotubes was enhanced by 94 %. It is considered that the CdS loaded N-doped TiO₂ NTs exhibited a significant synergistic effect resulting in the improvement of the photocatalytic capability in degrading MO dye under visible light irradiation. In short, oxygen vacancies and surface units [Ti⁴⁺-N³⁻] exist in the N-doped TiO₂ NTs [32]. Besides, the photogenerated electrons and holes can be separated effectively because of the charge-transfer process between CdS and TiO₂ [33].

Acknowledgements

This work was financially supported by the National Natural Science Foundation of China (Grant No. 21403184), the Natural Science Foundation of the Jiangsu Higher Education Institutions of China (Grant No. 14KJB150025 and 15KJB430032) and the China Postdoctoral Science Foundation (No. 2014M561622).

References

- [1] WANG Y., YU J., XIAO W., LI Q., *J. Mater. Chem. A*, 11 (2014), 3847.
- [2] RANI S., SURI P., SHISHODIA P.K., MEHRA R.M., *Sol. Energ. Mat. Sol. C*, 12 (2008), 1639.
- [3] AN L., WANG G., CHENG Y., GAO F., CHENG, Y., *J. Phys. Chem.*, 10 (2015), 1878.
- [4] WANG B., ZHANG G., SUN Z., ZHENG S., *Powder Technol.*, 262 (2014), 1.
- [5] WOJCIESZAK D., MAZUR M., KURNATOWSKA M., KACZMAREK D., DOMARADZKI J., KEPINSKI L., CHOJNACKI K., *J. Photoenergy*, 3 (2014), 591.
- [6] MOR G.K., VARGHESE O.K., PAULOSE M., SHANKAR K., GRIMES C.A., *Sol. Energ. Mat. Sol. C*, 14 (2006), 2011.
- [7] LI G., WU L., LI F., XU, P., ZHANG, D., LI, H., *Nanoscale*, 5 (2013), 2118.
- [8] DIWALD O., THOMPSON T.L., ZUBKOV T., YATES J.T.J., *J. Phys. Chem. B*, 19 (2004), 6004.
- [9] HUO K., GAO B., FU J., ZHAO L., CHU P.K., *Rsc Adv.*, 33 (2014), 17300.
- [10] PISKUNOV S., LISOVSKI O., BEGENS J., BOCHAROV D., ZHUKOVSKII Y.F., WESSEL M., *J. Phys. Chem. C*, 119 (2015), 18686.
- [11] BARAN E., YAZICI B., *J. Hydrogen Energ.*, 41 (4) (2016), 2498.
- [12] GOPINATH K., KUMARAGURU S., BHAKYARAJ K., ARUMUGAM A., *Superlattice. Microst.*, 92 (2016), 100.
- [13] AMPELLI C., GENOVESE C., LANZAFAME P., PERATHONER S., CENTI G., *Chem. Eng. Trans.*, 39 (2014), 1627.
- [14] XIAO F.X., MIAO J., WANG H.Y., LIU B., *J. Mater. Chem. A*, 39 (2013), 12229.
- [15] OUYANG J., CHANG M., ZHANG Y., LI X., *Thin Solid Films*, 7 (2012), 2994.
- [16] LI D., WANG S., WANG J., ZHANG X., LIU S., *Mater. Res. Bull.*, 10 (2013), 4283.
- [17] SUN L., CAI J., WU Q., HUANG P., SU Y., LIN C., *Electrochim. Acta*, 10 (2013), 525.
- [18] NOSAKA Y., MATSUSHITA M., NISHINO J., NOSAKA A., *Sci. Technol. Adv. Mat.*, 2 (2005), 143.
- [19] ANSARI S.A., *New J. Chem.*, 9 (2016), 558.
- [20] LI H., HAO Y., LU H., LIANG L., WANG Y.Y., QIU J.H., SHI X.C., WANG Y., YAO J.F., *Appl. Surf. Sci.*, 344 (2015), 112.
- [21] KIM D.H., HAN H.S., CHO I.S., SEONG W.M., PARK I.J., PARK J.H., SHIN S., DO PARK G., PARK S., LEE S., HONG K.S., *J. Hydrogen Energ.*, 1 (2015), 863.
- [22] LIU L., LV J., XU G., WANG Y., WANG Y., XIE K., *J. Solid State Chem.*, 12 (2013), 27.
- [23] LIANG Y., CUI Z., ZHU S., LIU Y., YANG X.J., *J. Catal.*, 278 (2011), 276.
- [24] KIM J.C., CHOI J., LEE Y.B., HONG J.H., LEE J.I., YANG J.W., LEE W.I., HUR N.H., *Chem. Commun.*, 48 (2006), 5024.
- [25] ZHANG, P., LIU, Y., TIAN, B., LUO, Y., ZHANG, J., *Catal. Today*, 281 (2017), 181.
- [26] YU S., HU J., LI J., *Int. J. Photoenergy*, 12 (2014), 1.
- [27] ZHANG S.S., PENG F., WANG H.J., YU H., ZHANG S.Q., YANG J., ZHAO H.J., *Catal. Commun.*, 8(2011), 689.
- [28] DANG M., ZHOU Y., LI H., LV C., *J. Mater. Sci. Mater. El.*, 1 (2012), 320.
- [29] XIE Y., KUM J., ZHAO X., CHAO S.O., *Semicond. Sci. Tech.*, 8 (2011), 5023.
- [30] PANT B., BARAKAT N.A.M., PANT H.R., PARK M., SAUD P.S., KIM J.W., KIM H.Y., *J. Colloid Interf. Sci.*, 434 (2014), 159.
- [31] LAN M., ZHANG Y., WANG P.N., *Chem. Phys. Lett.*, 4–6 (2008), 341.
- [32] ZHAO W., BAI Z., REN A., GUO B., WU C., *Appl. Surf. Sci.*, 11 (2010), 3493.
- [33] TANG J.W., ZOU Z.G., A, YE J.H., *Chem. Mater.*, 9 (2004), 1644.

Received 2016-08-12
Accepted 2018-05-02